# PHYSICAL MODELS FOR EVALUATING THE INTERFEROMETRIC COHERENCE OF POTENTIAL PERSISTENT SCATTERERS

*Gerardo Di Martino, Antonio Iodice, Davod Poreh, Daniele Riccio, Giuseppe Ruello*
Dipartimento di Ingegneria Elettrica e delle Tecnologie dell'Informazione,
Università di Napoli Federico II, 80125, Naples, Italy

## ABSTRACT

We present a model-based approach aimed to help predicting which objects in an imaged scene will appear as persistent scatterers in Differential Synthetic Aperture Radar Interferometry (DInSAR) data, given their shapes and sizes, and given the scene background and sensor parameters. The approach consists in computing the interferometric coherence of a pair of acquisitions for a resolution cell comprising a strong scatterer (trihedral or dihedral corner reflector, or metallic vertical cylinder) and a distributed scatterer (rough surface, vegetation).

***Index Terms***— Synthetic Aperture Radar (SAR), Differential SAR Interferometry, electromagnetic models, radar cross section.

## 1. INTRODUCTION

Differential Synthetic Aperture Radar Interferometry (DInSAR) is a powerful technique, able to measure very small movements of the terrain over time [1-4]. Different implementations of this technique are available [2-4], and one of the most popular is the the "permanent" (or "persistent", or "point-like") scatterer (PS) approach [3]. This approach focuses on the phase history of a limited number of very highly coherent pixels, corresponding to scene point-like elements having a greatly stable electromagnetic scattering behaviour over time and over incidence angle; this allows to employ very large sets of SAR acquisitions, also with very large temporal and spatial "baselines" (i.e., temporal and spatial separations among acquisition orbits); accordingly, a very high accuracy on the measured movement velocity of the selected points can be obtained. However, it is usually very difficult to understand which physical object (if any) corresponds to a given detected PS, even after a direct inspection of the imaged scene. Ray-tracing techniques have been employed to help identifying physical objects corresponding to PS, highlighting the importance of multiple reflections [5]. However, no quantitative study is available to quantitatively predict the coherence of pixels containing a potential PS. Only qualitative considerations have been made, which can be summarized as follows. Physical structures forming right-angle trihedral corners (for instance, windows' corners or balconies on building façades, or other man-made structures, such as bridge structural elements), or vertical cylinders on a horizontal plane (for instance, metallic poles or cylindrical tanks or silos), or right-angle dihedral corners aligned along the sensor line of flight (vertical walls on the ground, or again elements of building façades) usually act as PS because:

1) Their backscattering is high, so that their return is dominant with respect to the other scatterers within the same SAR resolution cell;
2) Their backscattering is stable over time, and this, together with point 1), leads to a very high temporal correlation coefficient ($\rho_{temp} \cong 1$);
3) Their backscattered signal is temporally concentrated in a very short time (ideally, in a single time instant), so that their range size is negligible and this, together with point 1), leads to a very high baseline correlation coefficient ($\rho_{bas} \cong 1$).

In this work, we try to put above considerations on a more quantitative footing by analytically evaluating the interferometric coherence of a pair of acquisitions for a resolution cell comprising one of the above described strong scatterers and a distributed scatterer (rough surface, vegetation). The obtained expression is provided as a function of scatterer shape and size, and of scene background and sensor parameters, so that it allows to predict if the considered strong scatterer will appear as a PS.

## 2. THEORY

Let us consider a resolution cell containing a strong point-like scatterer and a distributed scatterer. The signal $y_i$ received by the sensor in the *i*-th acquisition of the interferometric time series can be written as:

$$y_i = s_i + d_i \tag{1}$$

where $s_i$ is the (complex) deterministic return from the strong scatterer, whose square modulus is the scatterer's radar cross section (RCS) $\sigma_S$, and $d_i$ is the return from the distributed scatterer, which is assumed to be a zero-mean

complex circular Gaussian random variable, whose mean square modulus is equal to the distributed scatterer's normalized radar cross section (NRCS) $\sigma_D^0$ multiplied by the resolution cell area $A_r$. The correlation coefficient $\rho_{ij}$ of the generic interferometric pair of acquisitions $i$ and $j$ can be then expressed as

$$\rho_{ij} = \frac{\langle y_i y_j^* \rangle}{\sqrt{\langle |y_i|^2 \rangle \langle |y_j|^2 \rangle}} = \frac{e^{i\varphi_{ij}} \sigma_S + \rho_{Dij} \sigma_D^0 A_r}{\sigma_S + \sigma_D^0 A_r} =$$

$$= e^{i\varphi_{ij}} \frac{1 + e^{-i\varphi_{ij}} \rho_{Dij} SBR^{-1}}{1 + SBR^{-1}} \quad , \qquad (2)$$

where $\varphi_{ij}$ is the deterministic interferometric phase of the strong point-like scatterer, $\rho_{Dij}$ is the correlation coefficient of the distributed target and *SBR* is the signal-to-background ratio, defined as

$$SBR = \frac{\sigma_S}{\sigma_D^0 A_r} \quad . \qquad (3)$$

If, as it is often (but not always) the case, $|\rho_{Dij}| \ll 1$, then we have

$$|\rho_{ij}| \cong \frac{1}{1 + SBR^{-1}} \quad . \qquad (4)$$

The RCS of right-angle triherdal corner reflectors, or of right-angle dihedral corner reflectors aligned along the SAR line of flight, of linear size $L$ (see Fig. 1a-c) is given by [6]

$$\sigma_S = a \frac{4\pi L^4}{\lambda^2} \quad , \qquad (5)$$

where $\lambda$ is the wavelength and $a$ is a dimensionless constant of the order of unity that depends on corner shape and material, and is almost independent of the incidence angle. Some examples of values of $a$ are reported in Table I. The RCS of a metallic cylinder of radius $r$ and height $h$ on a horizontal plane (see Fig. 1d) is [6]

$$\sigma_S = \frac{8\pi r h^2}{\lambda} \quad . \qquad (6)$$

With regard to the NRCS of distributed targets, it may strongly vary based on the scatterers physical properties: for instance, for a soil rough surface it depends on soil complex dielectric constant and surface roughness [7], whereas for a vegetated area it depends on vegetation height, shape, density, etc. [7]. In most cases, at the intermediate incidence angles of interest for SAR systems, the NRCS of such distributed targets vary from 0.01 (-20 dB) to 1 (0 dB) [7]. Accordingly, the SBR can be expressed as

$$SBR = a' \frac{L^4}{\lambda^2 A_r} \qquad (7)$$

for trihedral or diherdral corners, and as

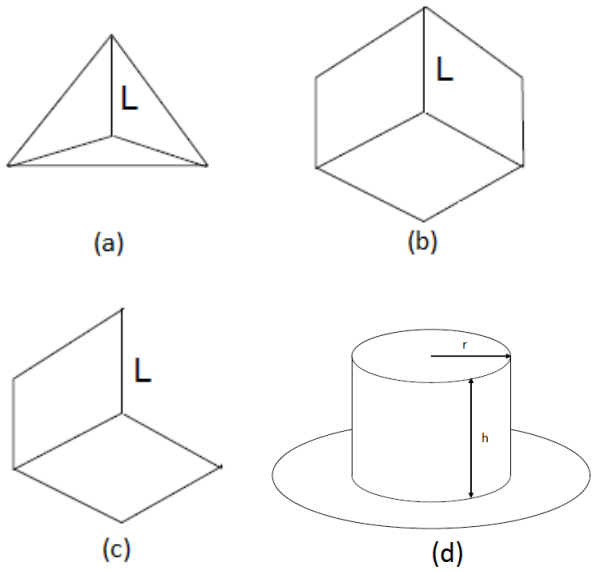


**Figure 1:** Triangular (a) and square (b) trihedral corners, dihedral corner (c), and metallic cylinder on a horizontal plane (d).

$$SBR = b \frac{r h^2}{\lambda A_r} \qquad (8)$$

for a metallic cylinder, where *a'* and *b* are dimensionless constants of a magnitude order varying from about 10 to about 1000, mainly depending on the NRCS of the distributed target. Equations (7) and (8) clearly show that, for a fixed scenario, SBR, and hence coherence, increase as operating frequency increases and as sensor resolution improves. This is in agreement with the well-known fact that PS density is greater in high-resolution X-band SAR sensors, such as Cosmo/SkyMed or TerraSAR-X, than in low- and medium-resolution C-band SAR sensors, such as Envisat or Sentinel-1.

Conversely, for a fixed sensor and a fixed background distributed target, the coherence increases as the linear size of the strong scatterer increases.

**Table I:** Values of the constant *a* for trihedral and dihedral corner scatterers.

| Target | *a* |
|---|---|
| Triangular trihedral corner | 1/3 |
| Square trihedral corner | 3 |
| Dihedral corner | 2 |

## 3. NUMERICAL RESULTS

Let us first illustrate the dependence of interferometric coherence of a potential PS on resolution. In Fig. 2 we plot the modulus of the correlation coefficient, computed via (4) and (7), as a function of resolution (i.e, the square root of $A_r$), for a trihedral corner with $L$ = 30 cm and $a'$ = 100, and wavelengths corresponding to X-, C- and L-band SAR sensors. By assuming a threshold of 0.9 for PS selection, the potential PS will be selected only for resolutions smaller than about 2, 6 and 10 m at L, C and X band, respectively, so that, for instance, it would be selected by using Cosmo/SkyMed or TerraSAR-X stripmap data, but not using Sentinel-1 interferometric mode data.

Let us now analyze the effect of scatterer size for a fixed sensor and background distributed target. To this aim, in Fig.3 we plot the modulus of the correlation coefficient of a trihedral corner, computed via (4) and (7), as a function of its linear size $L$ for $a'$ = 100 and for wavelengths and resolutions similar to those of Cosmo/SkyMed and Sentinel-1 SAR sensors. By assuming, again, a threshold of 0.9 for PS selection, the potential PS will be selected only if its size is larger than about 15 cm and about 40 cm for the Cosmo/SkyMed and Sentinel-1 SAR sensors, respectively.

Up to now we have assumed that the correlation coefficient of the background distributed target is negligible, as it is usually the case for vegetated areas. Let us now remove this assumption and analyze the effect of a non-negligible coherence of the distributed target. It must be noticed that the corresponding overall correlation, obtained by computing the modulus of (2), depends not only on the modulus of the distributed target correlation coefficient, but also on its phase. If the strong scatterer is very near to the distributed one (for instance, the strong scatterer is placed on the ground), the distributed target correlation coefficient is in phase with the strong scatterer's return (i.e., its phase is equal to $\varphi_{ij}$), and the overall correlation increases with respect to the one obtained in the case of incoherent background. However, sometimes, due to layover, the strong scatterer may by physically far from the distributed one, although belonging to the same SAR resolution cell: this is, for instance, the case of a strong scatterer placed on a tall building's façade at a high elevation, which belongs to the same resolution cell of the ground in front of the building. In this case, the distributed target correlation coefficient may be out of phase with the strong scatterer's return, and the overall correlation may be even smaller than the one obtained in the case of incoherent background. To illustrate this effect, in Fig. 4 we show the modulus of the overall correlation coefficient as a function of the SBR for different values of the modulus of the distributed target correlation coefficient, for both the in-phase and counter-phase cases.

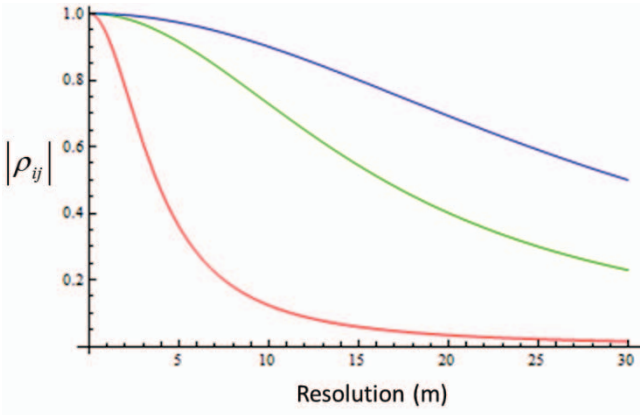


**Figure 2:** Modulus of the correlation coefficient as a function of resolution (i.e, the square root of $A_r$), for a trihedral corner with $L$ = 30 cm and $a'$ = 100, and for $\lambda$=3 cm (blue line), $\lambda$=5.5 cm (green line), and $\lambda$=24 cm (red line).

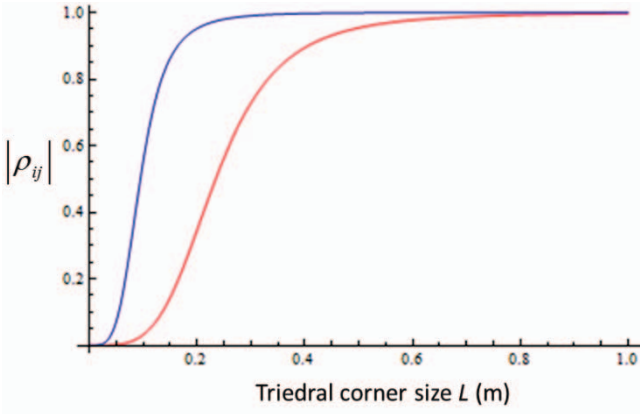


**Figure 3:** Modulus of the correlation coefficient of a trihedral corner as a function of its linear size $L$, for $a'$ = 100. Blue line: $\lambda$=3 cm, resolution = 3 m. Red line: $\lambda$=5.5 cm, resolution = 10 m.

## 4. CONCLUSIONS

We have presented a model-based approach that allows us computing the interferometric coherence of a pair of acquisitions for a resolution cell comprising a strong scatterer (trihedral or dihedral corner reflector, or meta*llic vertical cylinder*) and a distributed scatterer (rough surface, vegetation). Theory is complemented by numerical results.

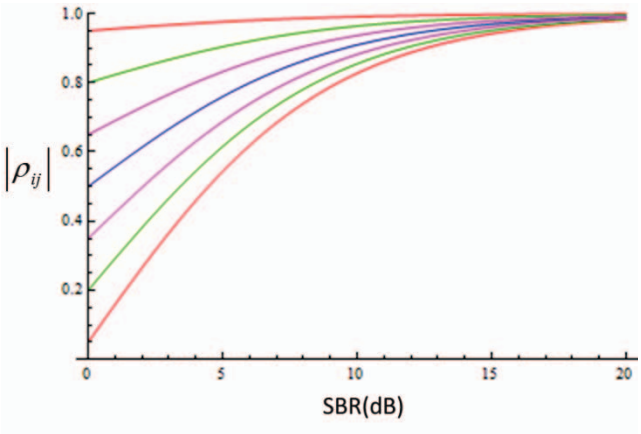


**Figure 4:** Modulus of the overall correlation coefficient as a function of the SBR when the modulus of the distributed target correlation coefficient is equal to: 0 (blue line), 0.3 (pink lines), 0.6 (green lines), 0.9 (red lines). Top lines: distributed target correlation coefficient is in phase with the strong scatterer's return. Bottom lines: distributed target correlation coefficient is in counter-phase with the strong scatterer's return.

## 5. REFERENCES

[1] A. K. Gabriel, R. M. Goldstein, and H. A. Zebker, "Mapping small elevation changes over large areas: Differential interferometry", *J. Geophys. Res.,* vol.94, pp. 9183-9191, 1989.

[2] A. Iodice, "A Survey of Differential SAR Interferometry for Surface Displacement Monitoring", *Proceedings of the 6th European Radar Conference,* pp. 212-214, Rome (Italy), 2009.

[3] A. Ferretti, C. Prati, F. Rocca, "Permanent scatterers in SAR interferometry", *IEEE Transactions on Geoscience and Remote Sensing*, Vol. 39, No.1, pp. 8-20, 2001.

[4] P. Berardino, G. Fornaro, R. Lanari, E. Sansosti, "A new algorithm for surface deformation monitoring based on small baseline differential SAR interferograms", *IEEE Transactions on Geoscience and Remote Sensing*, Vol. 40, No.11, pp. 2375-2383, 2002.

[5] S. Auer, S. Gernhardt, R. Bamler, "Investigations on the Nature of Persistent Scatterers Based on Simulation Methods", *Proceedings of the Joint Urban Remote Sensing Event, JURSE 2011,* pp. 61 – 64, Munich (Germany), 2011.

[6] G. T. Ruck, D. E. Barrick, W. D. Stuart, C. K. Krichbaum, *Radar Cross Section Handbook*, Vol. 2, Plenum Press, 1970.

[7] F. T. Ulaby, R. K. Moore, and A. K. Fung, *Microwave Remote Sensing*, Vol. II, Reading, MA: Addison-Wesley, 1982.